

Suppression of Ion-Scale Microtearing Modes by Electron-Scale Turbulence via Cross-Scale Nonlinear Interactions in Tokamak Plasmas

S. Maeyama* and T.-H. Watanabe

Department of Physics, Nagoya University, Nagoya 464-8602, Japan

A. Ishizawa

Kyoto University, Gokasho, Uji, Kyoto 611-0011, Japan

(Received 12 July 2017; published 9 November 2017)

Gyrokinetic turbulence simulations are applied for the first time to the cross-scale interactions of microtearing modes (MTMs) and electron-temperature-gradient (ETG) modes. The investigation of the fluctuation response in a multiscale simulation including both types of instabilities indicates that MTMs are suppressed by ETG turbulence. A detailed analysis of nonlinear mode coupling reveals that radially localized current-sheet structures of MTMs are strongly distorted by fine-scale $\mathbf{E} \times \mathbf{B}$ flows of ETG turbulence. Consequently, electron heat transport caused by the magnetic flutter of MTMs is significantly reduced and ETG turbulence dominates electron heat transport.

DOI: 10.1103/PhysRevLett.119.195002

Introduction.—Since magnetic fusion plasmas experience a wide variety of modes of fluctuation, plasma turbulence involving multiple spatiotemporal-scale instabilities has emerged as a key issue to be addressed in fusion science [1]. Owing to the advancement in high-performance computing technologies and algorithms, gyrokinetic simulations are now a powerful tool for investigating multiscale plasma turbulence. Direct numerical simulations of multiscale plasma turbulence covering both short wavelength electron-scale and long wavelength ion-scale fluctuations (with scales characterized by their gyroradii ρ) clarify the cross-scale interactions between electron and ion temperature gradient modes (ETG/ITG) in tokamaks [2–4]. Comparisons between simulations and experiments show that in several magnetic fusion devices, cross-scale interactions are necessary for explaining experimental transport levels and are relevant for ITER-baseline parameters [5–7]. Multiscale physics including electron-scale dynamics has drawn attention not only in fusion science but also in the astrophysics associated with solar-wind turbulence [8] and magnetic reconnection [9].

Our recent work revealed the mechanism of cross-scale interaction in multiscale ETG/ITG turbulence via intermediate (sub-ion-scale) structures, where we found shearing of ETG fluctuations by ITG turbulence eddies, as well as the generation of ITG-driven short wavelength zonal flows and their damping by ETG turbulence [4,10]. However, because of the huge computational complexity involved, analysis of multiscale turbulence has been limited to the cases of ETG and ITG turbulence. Application of multiscale gyrokinetic simulations to other cases is a critical step for extending our understanding of the multiscale nature of magnetized-plasma turbulence. Extracting common features of multiscale turbulence will help

constructing a simple model for cross-scale interactions (early attempts are found, e.g., in Refs. [11,12]), and will draw directions for future theoretical studies.

In this Letter, we first apply a multiscale analysis to ETG and microtearing-mode (MTM) turbulence. Whereas ETGs are essentially electrostatic, MTMs, that is, a kinetic extension of MHD tearing modes, are electromagnetic instabilities and driven by the electron temperature gradient [13]. They have been considered as candidates for driving electron heat transport in tokamak cores [14], spherical tokamaks [15], and *H*-mode pedestals [16,17]. The linear eigenfunction of an MTM typically comprises a poloidal wavelength of the order of ion acoustic gyroradius ρ_a , and forms a radially localized current-sheet structure much thinner than ρ_a around mode-rational surfaces where the parallel wave number k_{\parallel} approaches zero in a sheared magnetic geometry. Therefore, our finding from the multiscale ETG/ITG turbulence study [4], summarized as “electron-scale turbulence can effectively interact with sub-ion-scale structures,” motivates us to investigate whether ETG turbulence affects MTMs. A deeper understanding of ETG and MTM turbulence is important not only for theoretical interest but also for resolving critical issues related to the ITER performance prediction and electron transport in spherical tokamaks. Gyrokinetic simulations in the present study reveal that the ETG suppresses the MTM fluctuations by destroying radially localized current sheets, thereby significantly affecting electron heat transport. This suggests that a paradigm shift from single-scale [16,17] to multiscale analysis may be necessary for ITER pedestal prediction, and that the electron heat transport in spherical tokamaks is determined through the interactions between ETG and MTM.

Simulation model.—Massively parallelized simulations of multiscale ETG/MTM turbulence have been performed

using the gyrokinetic Vlasov simulation code GKV [18,19], which solves the electromagnetic gyrokinetic equations in a flux-tube limit. Employed plasma parameters are like an ASDEX-Upgrade *H*-mode discharge AUG#29224 at mid radius [20]: the ratios of major radius to the density and electron temperature scale lengths $R/L_n = 0.26$ and $R/L_{T_e} = 5.9$, the inverse aspect ratio $\epsilon = r/R = 0.19$, the safety factor $q = 1.34$, the magnetic shear $\hat{s} = 1.0$, the electron-to-deuterium mass ratio $m_e/m_i = 1/3672$, the electron-to-ion temperature ratio $T_e/T_i = 1.0$, and the normalized collisionality $\nu_e^* = qR\nu_{ee}/(\sqrt{2}\epsilon^{3/2}v_{te}) = 0.052$, respectively. Apart from the experimental values, we set a higher plasma beta value $\beta = 2\mu_0 n_0(T_e + T_i)/B^2 = 6.0\%$ and the ion temperature gradient to zero, $R/L_{T_i} = 0$, so as to focus on interactions between ETG and MTM turbulence, while keeping the ITG modes stable, and employ a simplified magnetic equilibrium (an $s - \alpha$ geometry) and a Lenard-Bernstein collision operator. A corresponding linear dispersion relation is plotted in Fig. 1(a), where the ETG modes are unstable for $k_y\rho_a > 5$ and the unstable modes appearing for $k_y\rho_a < 1$ are the MTMs, which are characterized by the tearing parity of the mode structure $\phi(-x, y, -z) = -\phi(x, y, z)$ and $A_{\parallel}(-x, y, -z) = A_{\parallel}(x, y, z)$ [21]. Here, x , y , and z denote the radial, field-line label, and field-aligned coordinates, respectively. Although trapped electron modes are known as an alternative candidate for driving electron transport [22], they are not unstable for this plasma parameter. To examine the effects of ETG turbulence upon MTMs with finite amplitudes, we have carried out two nonlinear simulations: a “low- k ” simulation resolving only MTM turbulence and a “full- k ” simulation resolving both ETG and MTM turbulence. Both of the simulations are carried out with the same simulation box of $-20\rho_a \leq x < 20\rho_a$, $-31.4\rho_a \leq y < 31.4\rho_a$, $-\pi \leq z < \pi$, $-4v_{ts} \leq v_{\parallel} \leq 4v_{ts}$, and $0 \leq \mu \leq 8T_s/B$, where v_{\parallel} and μ denote the parallel velocity and the magnetic moment, respectively. The low- k simulation has a coarser resolution with $512 \times 64 \times 48 \times 64 \times 16$ grid points in order of $(x, y, z, v_{\parallel}, \mu)$, while the full- k simulation achieves a finer perpendicular-space resolution with $1024 \times 1024 \times 48 \times 64 \times 16$ grid points. The initial values of the full- k simulation are given by the result of the low- k simulation in a steady turbulent state with zero padding for the high- k components. Therefore, deviations of the full- k simulation from the low- k simulation arise from the effects of ETG upon MTMs, and vice versa.

Simulation results.—Figure 1(b) shows the time evolution of the electron heat fluxes $Q_{eE} = \sum_k \text{Re}[-ik_y \tilde{\phi}_k \tilde{p}_{ek}^*/B]$ and $Q_{eM} = \sum_k \text{Re}[ik_y \tilde{A}_{\parallel k} \tilde{q}_{e\parallel k}^*/B]$, which are caused by $\mathbf{E} \times \mathbf{B}$ flows and magnetic flutter, respectively, where \tilde{p}_e and $\tilde{q}_{e\parallel}$ denote the perturbed electron pressure and the parallel heat flux and $\langle \dots \rangle$ denotes a volume average. In the low- k simulation, the MTM instability linearly grows with the time scale on the order of $\gamma_{l, \text{MTM}}^{-1} \sim 10R/c_a$, and the electron heat

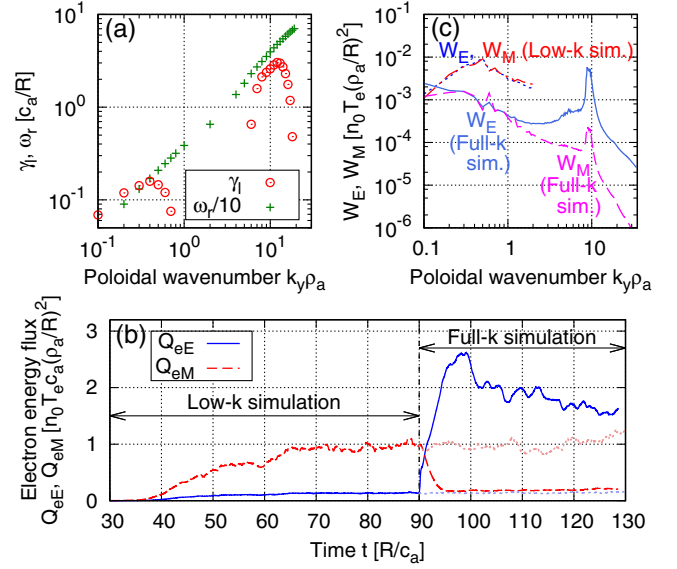


FIG. 1. (a) Linear growth rate γ_l and real frequency ω_r as functions of the poloidal wave number k_y . (b) Time evolution of the electron heat flux caused by $\mathbf{E} \times \mathbf{B}$ flows and magnetic flutter, Q_{eE} and Q_{eM} . We carried out a low- k simulation resolving only MTM ($k_y\rho_a \leq 2.1$) up to $t = 90R/c_a$, and then refined grid sizes as a full- k simulation resolving ETG/MTM ($k_y\rho_a \leq 34.1$). (c) Poloidal-wave-number spectra of the electrostatic and magnetic-field energies, W_{Ek} and W_{Mk} . Dotted (blue) and chain (red) lines plot results from the low- k simulation, while solid (cyan) and dashed (pink) lines correspond to the full- k simulation.

flux is mainly due to magnetic flutter. Refining the numerical grid in $x - y$ space, the full- k simulation starts from $t = 90R/c_a$. Here, the ETG instability rapidly grows, and then the electron heat flux is mainly driven by the $\mathbf{E} \times \mathbf{B}$ flows, where 96% of Q_{eE} is attributed to electron-scale fluctuations with $k_y\rho_a > 5$. At the same time, the heat flux caused by the magnetic flutter Q_{eM} (mainly driven by MTMs) is significantly suppressed by a factor of 5. While the full- k simulation is continued over several linear-growth times of $\gamma_{l, \text{MTM}}^{-1}$, the MTM does not reappear, in contrast to the previous result for multiscale simulation of ETG/ITG turbulence in which ITG instability grew even in the presence of ETG turbulence [4]. Field energy spectra obtained from the gyrokinetic simulations are shown in Fig. 1(c). The electrostatic and magnetic-field energies are, respectively, given by $W_E = \sum_k \text{Re}[\{\epsilon_0 k_{\perp}^2 + \sum_s (e_s^2 n_s / T_s)(1 - \Gamma_{0sk})\} |\tilde{\phi}_k|^2 / 2]$ and $W_M = \sum_k \text{Re}[k_{\perp}^2 |\tilde{A}_{\parallel k}|^2 / (2\mu_0)]$, and averaged over $65 < tc_a/R < 85$ for the low- k simulation and over $105 < tc_a/R < 125$ for the full- k simulation. During the low- k simulation, the saturation levels of W_E and W_M are comparable because of the shear-Alfvénic nature of the MTM turbulence. On the other hand, in the full- k simulation, ETG turbulence becomes dominant and W_E peaks at an electron scale of $k_y\rho_a \approx 9$, where $W_E \gg W_M$ due to the electrostatic properties of ETG. Compared to the low- k case, the field energy for $k_y\rho_a \leq 2.1$ is significantly reduced by a factor of 5,

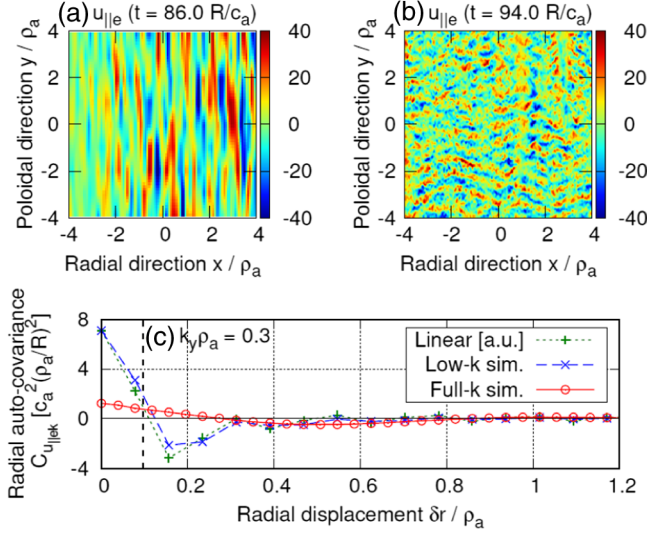


FIG. 2. Structure of the electron-parallel current, $u_{||e}$. Snapshots in the midplane of flux-tube $\theta = 0$ (a) in the low- k simulation, $t = 86R/c_a$, and (b) in the full- k simulation, $t = 94R/c_a$. (c) Radial autocovariance of $u_{||e}$ for the $k_y \rho_a = 0.3$ mode of MTM. Dotted (green), dashed (blue), and solid (red) lines correspond to the linear eigenfunction, the low- k simulation, and the full- k simulation, respectively. A linear theoretical estimate, $\delta r_{\text{est}} = \pm 0.096 \rho_a$, is also plotted.

which is consistent with the reduction of the electron heat flux caused by magnetic flutter, as shown in Fig. 1(b). Thus, the simulation suggests that ETG turbulence can suppress MTM and dominate electron heat transport.

To discuss the suppression of MTMs, we examine the structures of the parallel electron current $u_{||e}$. As shown in the low- k simulation, Fig. 2(a), MTM turbulence is accompanied by radially localized current-sheet structures with wavelengths that are characterized by the ion-acoustic gyroradius, ρ_a , in the y direction, but which are much shorter in the x direction. Figure 2(b) shows the disappearance of the MTM current-sheet structure in the full- k simulation due to the ETG turbulence with $k_y \rho_a \approx 9$ (or $\lambda_y \approx 0.7 \rho_a$). To evaluate the MTM current-sheet width more quantitatively, the radial auto-covariance of the electron parallel current,

$$C_{u_{||ek}}(\delta r) = \text{Re}[\langle u_{||ek_y}(x, z) u_{||ek_y}^*(x + \delta r, z) \rangle], \quad (1)$$

is computed for a typical MTM of $k_y \rho_a = 0.3$, as shown in Fig. 2(c). The current-sheet width of a linear MTM is measured by the radial correlation length, $\delta r \approx 0.1 \rho_a$, and is consistent with a theoretical estimate for the electron-resonance condition near the $k_{||} \approx 0$ surface [23]; namely, $\delta r_{\text{est}} = qR\omega / (\hat{s} k_y v_{te}) = 0.096 \rho_a$ for $k_y \rho_a = 0.3$ and $\omega = 1.31 c_a / R$. The current-sheet width under low- k MTM turbulence is also similar to that of the linear MTM. In contrast, the amplitude of the radial auto covariance of electron current, $C_{u_{||ek}}$, is reduced in the full- k ETG/MTM

turbulence and its radial correlation length becomes longer than those in the linear and turbulent regimes of the MTM instabilities [Fig. 2(c)]. This implies that the radially localized current-sheet structures of the MTM are destroyed in the presence of ETG turbulence.

The nonlinear cross-scale interactions between ETG and MTM turbulence are investigated by means of sub-space-transfer analysis based on the gyrokinetic entropy balance, where the sub-space-transfer function of the electron entropy variable [10],

$$J_{ek}^{\Omega_i, \Omega_j} = \sum_{p \in \Omega_i} \sum_{q \in \Omega_j} J_{ek}^{p, q}, \quad (2)$$

is given by a partial sum of the triad-transfer function $J_{ek}^{p, q}$ over the subspaces Ω_i and Ω_j of the wave-number space.

The sub-space-transfer function $J_{ek}^{\Omega_i, \Omega_j}$ is regarded as the entropy gain or loss of the mode k through the coupling with the modes $p \in \Omega_i$ and $q \in \Omega_j$, and satisfies a symmetry condition, $J_{ek}^{\Omega_i, \Omega_j} = J_{ek}^{\Omega_j, \Omega_i}$, and a detailed balance relation, $\sum_{k \in \Omega_k} J_{ek}^{\Omega_i, \Omega_j} + \sum_{k \in \Omega_j} J_{ek}^{\Omega_k, \Omega_i} + \sum_{k \in \Omega_i} J_{ek}^{\Omega_j, \Omega_k} = 0$. See Ref. [10] for more details concerning the sub-space-transfer analysis; it may be treated as an anisotropic extension of triple-shell transfer [24]. Here, we employ a fluid approximation of the gyrokinetic entropy transfer to reduce the computational complexity and divide the wave-number space into two subspaces, i.e., a low- k_y subspace, $\Omega_L = \{k | k_y \rho_a \leq 2.1\}$, and a high- k_y subspace, $\Omega_H = \{k | k_y \rho_a > 2.1\}$. The two-dimensional subspace-transfer spectra are shown in Fig. 3, which clearly captures the nonlinear interactions responsible for the suppression of MTMs by ETG. First, we note that $J_{ek}^{\Omega_H, \Omega_H}$ has distinctive negative values for $k_y \rho_a < 1$ and $|k_x \rho_a| = 1-7.5$ in Fig 3(a); this means that low- k_y MTM turbulence is suppressed by the coupling with the high- k_y fluctuations of ETG. The broadened spectrum in the k_x direction reflects the radially localized current-sheet structures. Indeed, the spectra of field energy or electron density fluctuations in MTM turbulence have peaks around $k_x \approx 0$, whereas the parallel-electron-current fluctuations tend to show a broad spectrum in k_x . Because high- k_y ETG turbulence is almost electrostatic, $J_{ek}^{\Omega_H, \Omega_H}$ originates from the $\mathbf{E} \times \mathbf{B}$ nonlinearity but not from the magnetic flutter. Second, $2J_{ek}^{\Omega_L, \Omega_H}$ has positive values around $k_y \rho_a = 8-14$ and $|k_x \rho_a| = 2.5-10$ in Fig. 3(b), meaning that these modes obtain entropy by the coupling with ion- and electron-scale modes. The direction of the entropy transfer is determined by considering the detailed balance $\sum_{k \in \Omega_L} J_{ek}^{\Omega_H, \Omega_H} + \sum_{k \in \Omega_H} 2J_{ek}^{\Omega_L, \Omega_H} = 0$. The entropy lost from the $k_y \rho_a < 1$ and $|k_x \rho_a| = 1-7.5$ modes [negative values of $\sum_{k \in \Omega_L} J_{ek}^{\Omega_H, \Omega_H}$ in Fig 3(a)] is found to be transferred to the modes at $k_y \rho_a = 8-14$ and $|k_x \rho_a| = 2.5-10$ [positive values of $\sum_{k \in \Omega_H} 2J_{ek}^{\Omega_L, \Omega_H}$ in Fig 3(b)]

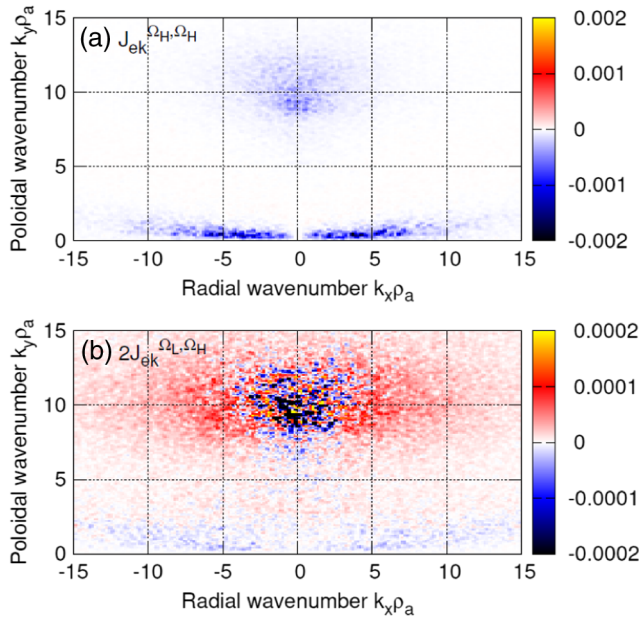


FIG. 3. 2D wave number spectra of nonlinear electron-entropy transfer during MTM suppression in the full- k simulation (snapshots at $t = 92.0R/c_a$): (a) the contribution by the high- k_y , high- k_x coupling $J_{ek}^{\Omega_L, \Omega_H}$; (b) the contribution by the low- k_y , high- k_x coupling $2J_{ek}^{\Omega_L, \Omega_H} = J_{ek}^{\Omega_L, \Omega_H} + J_{ek}^{\Omega_H, \Omega_L}$, as normalized by $n_0 T_e c_a \rho_a^2 / R^3$.

through a coupling with the modes satisfying the triad-coupling condition $\mathbf{k} + \mathbf{p} + \mathbf{q} = \mathbf{0}$, e.g., $|k_y \rho_a| \sim 9$ and $|k_x \rho_a| \sim 0$. In other words, low- k_y MTMs are broken into small-scale eddies by means of the shearing by high- k_y ETG turbulent $\mathbf{E} \times \mathbf{B}$ flows. It should also be noted that structures of radially localized MTM current sheets with low- k_y but high- k_x effectively interact with electron-scale turbulence.

Summary.—We have investigated the cross-scale interactions between electron-scale ETG turbulence and ion-scale MTM turbulence by means of electromagnetic gyrokinetic simulations. Numerical analysis of multiscale ETG/MTM turbulence showed that ETG turbulence stabilizes the MTMs. A detailed analysis of nonlinear mode coupling based on the subspace transfer of the electron-entropy variable revealed that components of the MTM turbulence with low k_y but high k_x were effectively regulated via coupling with electron-scale $\mathbf{E} \times \mathbf{B}$ flows, since radially localized current-sheet structures of the MTMs were strongly distorted by ETG turbulence. Thus, the electron heat transport was concluded to be mainly driven by electron-scale ETG turbulence. This suggests that cross-scale interactions between the electron and ion scales are directly related to the evaluation and modeling of turbulent transport. This result is important not only for tokamak-core ETG/ITG turbulence, but also for transport in a spherical tokamak or in an H -mode pedestal, where MTM and ETG instabilities may coexist.

Finally, let us discuss commonalities between the results of this Letter and those of previous studies on multiscale ETG/ITG turbulence [4,10] to establish comprehensive understandings of cross-scale interactions in multiscale plasma turbulence. In both cases, we emphasize the importance of sub-ion-scale structures (i.e., intermediate scales between the ion and electron scales) for cross-scale coupling. There are, for example, short wavelength ITG eddies or short wavelength zonal flows in the ETG/ITG turbulence, as well as radially localized MTM-current sheets in the ETG/MTM turbulence. MTMs having high- k_x structures as linear eigenfunctions will readily interact with ETG turbulence. This may be why ITG can linearly grow in the presence of ETG turbulence, whereas MTMs cannot. Parameter scans of multiscale ETG/MTM turbulence are desirable for clarifying the conditions under which ETG dominates MTM or the possibility of nonlinear drive of MTM [25]. For example, the ratio of the ETG and MTM linear growth rates can be controlled by the plasma beta value or magnetic shear. Additionally, a longer time scale simulation than that in this study ($\sim 40R/c_a = 6374a/v_{te}$, where the minor radius $a = 0.38R$) may also be required, since a recent study on ETG turbulence with adiabatic ion model reported that slowly developed ($\sim 10^4 a/v_{te}$) electron-scale zonal flow can suppress ETGs [26]. However, these issues demand extreme computational resources, and, therefore, remain for future work.

S. M. acknowledges fruitful discussions with Dr. Y. Idomura and Dr. H. Doerk. This work was supported by MEXT FLAGSHIP 2020 project as a priority issue on Post-K computer (Category 6-D), MEXT KAKENHI Grants No. 26800283 and No. 17K14424. Computations were performed on K at RIKEN-AICS through HPCI System Research Project (ID: hp160208, hp170075), FX100 at Nagoya University through JHPCN Research Project (ID: jh160028, jh170020), and Plasma Simulator at NIFS.

*smaeyama@p.phys.nagoya-u.ac.jp

- [1] A. Fasoli, S. Brunner, W. A. Cooper, J. P. Graves, P. Ricci, O. Sauter, and L. Villard, *Nat. Phys.* **12**, 411 (2016).
- [2] J. Candy, R. E. Waltz, M. R. Fahey, and C. Holland, *Plasma Phys. Controlled Fusion* **49**, 1209 (2007).
- [3] T. Görler and F. Jenko, *Phys. Rev. Lett.* **100**, 185002 (2008).
- [4] S. Maeyama, Y. Idomura, T.-H. Watanabe, M. Nakata, M. Yagi, N. Miyato, A. Ishizawa, and M. Nunami, *Phys. Rev. Lett.* **114**, 255002 (2015).
- [5] N. T. Howard, C. Holland, A. E. White, M. Greenwald, and J. Candy, *Phys. Plasmas* **21**, 112510 (2014).
- [6] N. Bonanomi, and P. Mantica *et al.*, *Proceedings of the 26th IAEA Fusion Energy Conference*, EX/P6-14 (2016).
- [7] C. Holland, N. T. Howard, and B. A. Grierson, *Nucl. Fusion* **57**, 066043 (2017).
- [8] C. H. K. Chen, S. Boldyrev, Q. Xia, and J. C. Perez, *Phys. Rev. Lett.* **110**, 225002 (2013).

- [9] J. L. Burch *et al.*, *Science* **352**, aaf2939 (2016).
- [10] S. Maeyama, T.-H. Watanabe, Y. Idomura, M. Nataka, A. Ishizawa, and M. Nunami, *Nucl. Fusion* **57**, 066036 (2017).
- [11] S. I. Itoh and K. Itoh, *Plasma Phys. Controlled Fusion* **43**, 1055 (2001).
- [12] C. Holland and P. H. Diamond, *Phys. Plasmas* **11**, 1043 (2004).
- [13] R. D. Hazeltine, D. Dobrott, and T. S. Wang, *Phys. Fluids* **18**, 1778 (1975).
- [14] H. Doerk, F. Jenko, M. J. Pueschel, and D. R. Hatch, *Phys. Rev. Lett.* **106**, 155003 (2011).
- [15] W. Guttenfelder, J. Candy, S. M. Kaye, W. M. Nevins, E. Wang, R. E. Bell, G. W. Hammett, B. P. LeBlanc, D. R. Mikkelsen, and H. Yuh, *Phys. Rev. Lett.* **106**, 155004 (2011).
- [16] D. Dickinson, C. M. Roach, S. Saarelma, R. Scannell, A. Kirk, and H. R. Wilson, *Phys. Rev. Lett.* **108**, 135002 (2012).
- [17] D. R. Hatch, M. Kotschenreuther, S. Mahajan, P. Valanju, F. Jenko, D. Told, T. Görler, and S. Saarelma, *Nucl. Fusion* **56**, 104003 (2016).
- [18] T.-H. Watanabe and H. Sugama, *Nucl. Fusion* **46**, 24 (2006).
- [19] S. Maeyama, T.-H. Watanabe, Y. Idomura, M. Nakata, M. Nunami, and A. Ishizawa, *Parallel Comput.* **49**, 1 (2015).
- [20] H. Doerk, M. Dunne, F. Jenko, F. Ryter, P. A. Schneider, E. Wolftrum, and T. A. U. Team, *Phys. Plasmas* **22**, 042503 (2015).
- [21] A. Ishizawa, S. Maeyama, T.-H. Watanabe, H. Sugama, and N. Nakajima, *J. Plasma Phys.* **81**, 435810203 (2015).
- [22] D. Told, F. Jenko, T. Görler, F. J. Casson, E. Fable, and A. U. Team, *Phys. Plasmas* **20**, 122312 (2013).
- [23] J. W. Connor, S. C. Cowley, and R. J. Hastie, *Plasma Phys. Controlled Fusion* **32**, 799 (1990).
- [24] B. Teaca, A. B. Navarro, F. Jenko, S. Brunner, and L. Villard, *Phys. Rev. Lett.* **109**, 235003 (2012).
- [25] X. Garbet, F. Mourgues, and A. Samain, *Plasma Phys. Controlled Fusion* **32**, 131 (1990).
- [26] G. J. Colyer, A. A. Schekochihin, F. I. Parra, C. M. Roach, M. A. Bernes, Y. c. Ghim, and W. Dorland, *Plasma Phys. Controlled Fusion* **59**, 055002 (2017).